Obtaining the Bidirectional Transfer Distribution Function of Isotropically Scattering Materials Using an Integrating Sphere

Jacob C. Jonsson [a,*] Henrik Brandén [b]

[a] *Environmental Energy Technology Division, Lawrence Berkeley National Lab, 1 Cyclotron Rd MS70A-2255, Berkeley, CA 94720, U.S.A.*

[b] *Department of Scientific Computing, Information Technology, Uppsala University, Box 337, SE-751 05 Uppsala, Sweden.*

Abstract

This paper demonstrates a method to determine the bidirectional transfer distribution function (BTDF) using an integrating sphere. Information about the sample's angle dependent scattering is obtained by making transmittance measurements with the sample at different distances from the integrating sphere. Knowledge about the illuminated area of the sample and the geometry of the sphere port in combination with the measured data combines to an system of equations that includes the angle dependent transmittance.

The resulting system of equations is an ill-posed problem which rarely gives a physical solution. A solvable system is obtained by using Tikhonov regularization on the ill-posed problem. The solution to this system can then be used to obtain the BTDF.

Four bulk-scattering samples were characterised using both two goniophotometers and the described method to verify the validity of the new method. The agreement shown is great for the more diffuse samples. The solution to the low-scattering samples contains unphysical oscillations, but still gives the correct shape of the solution. The origin of the oscillations and why they are more prominent in low-scattering samples are discussed.

Key words: BTDF, light scattering, integrating sphere
PACS: 42.25.Fx, 07.60.-j, 07.60.Dq, 07.05.Kf, 02.60.Nm

* Corresponding author.
Email address: JCJonsson@lbl.gov (Jacob C. Jonsson).

1 Introduction

The method described in this paper is based on the simple observation that light scattered at high angles is not detected if the scattering sample is not in direct contact with the integrating sphere. The bidirectional transmittance distribution function (BTDF) is obtained by combining measurements when the sample is at different distances with a model for how much light is detected from each scattering angle for that distance.

The relationship between angle interval within which scattered light is detected and sample distance from the sphere port is a geometric problem. The relationship is trivial if the sample is illuminated by a dot at normal angle of incidence and in line with the center of the sphere port. However this simplified situation is rarely the case, as it is common that an area of the sample is illuminated to obtain a mean transmittance value for inhomogeneous samples.

Determination of the angular distribution of scattered light from materials is of interest for a variety of fields from macroscopic problems like daylighting simulations for buildings down to smaller scale situations such as light trapping in solar cells [1]. Obtaining material data of this kind has traditionally been done using a goniophotometer. Such instruments have been built and described by several research groups around the world, however, it is not a common, easily obtained instrument among materials manufacturers, producers and designers. The only organized inter-laboratory comparison of goniometer type instruments [2] showed that different instruments are not always in agreement. Spectrophotometers fitted with integrating spheres are on the other hand more common and available from several manufacturers, allowing for a larger probability to be able to obtain accurate and repeatable results in different laboratories.

2 Theory

Four key elements are needed to solve the given problem of obtaining the scattering behavior of a sample: 1. The definition of the BTDF which is the value that describes scattering for a sample. 2. A measurement technique to obtain information about the scattering distribution. 3. A model to describe how the measured values relate to the BTDF. 4. A method to solve the model.

2.1 Bidirectional scattering distribution function – BSDF

The Bidirectional Reflectance Distribution Function, BRDF, was defined by Nicodemus, [3,**?**] and a corresponding definition has been made for transmitted scattering as well [4]. In more general discussions that covers both transmitted and reflected scattering it is common to use the general term BSDF, Bidirectional Scattering Distribution Function. The BSDF describes a surface's or bulk sample's scattering properties with respect to all incoming and outgoing directions, this makes it a powerful tool for studying and comparing scattering materials.

Nicodemus originally gave the definition of the BRDF as the differential scattered radiance divided by the differential incident irradiance, however, Stover [5] argues that the use of non-differential quantities is more reasonable when working with experimental equipment and defines the BSDF as

$$\text{BSDF} \equiv \frac{P_s/\Omega_s}{P_i \cos\theta_s}, \tag{1}$$

where P_s is the scattered light flux (Watts), Ω_s is the solid angle into which the scattered light is redirected (sr), P_i is the incident light flux (Watts), θ_s is the scattering angle. The differential form is very similar

$$\text{BSDF} = \frac{dP_s/d\Omega_s}{P_i \cos\theta_s}. \tag{2}$$

The non-differential definition is also used in ASTM standard E1392 [6] (which has been taken over by the SEMI standard ME1392 [7]). The geometry is shown in Fig. 1. The definition can be explained by parts three parts: 1. The ratio between incoming and outgoing flux, P_s/P_i, which is classic from definitions of transmittance and reflectance. 2. The $1/\Omega_s$ which is needed to define the area of to where light is scattered. 3. The $1/\cos\theta_S$ term that models the projection of the solid angle with respect to the scattering surface. One can also look at the third term as a correction of the size of the illuminated area as seen from the solid angle [5].

Commonly the BSDF is written as dependent of four parameters, the incident angles (θ_i and ϕ_i) and the scattered angles(θ_s and ϕ_s). In reality the BSDF also depends on wavelength and polarization state of the incident light. Even more obvious, but easy to neglect, is that an inhomogeneous sample can have different properties over different areas, and must be considered "as is" when it come manufacturing, polishing, and any other treatments that might affect the samples scattering properties. Therefore it is recommended to use the BSDF more as a sample property than a pure materials property. With this

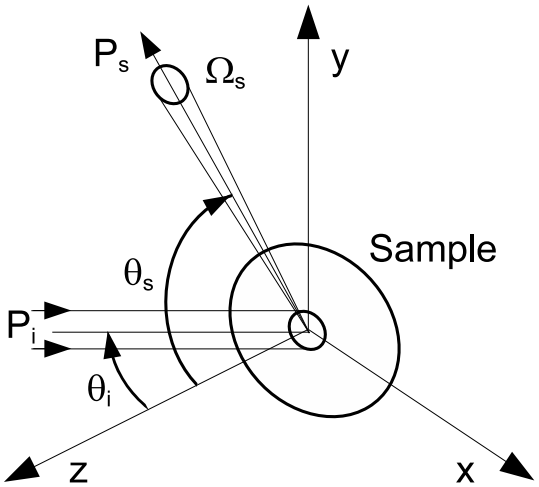

Fig. 1. The light incident at an angle θ_i is scattered from the sample at an angle θ_s. Incident and outgoing light fluxes are shown as P_i and P_s respectively, also the outgoing solid angle Ω_s.

in mind, it is still reasonable that samples manufactured and treated the same way should have the same BSDF.

It should be noted that the above definition is in radiometric units. It is also common to define the BSDF in photometric units as the luminance divided by the illuminance of the scatterer [8]. However, this paper uses radiometric units.

Of special relevance to this paper is the calculation of how the direct-hemispherical reflectance, ρ_{dh}, and transmittance, τ_{dh}, can be calculated using the BRDF [3,6,7] and BTDF [9]. The direct-hemispherical value describes how much light is reflected (or transmitted) in all outgoing angles (hemispherically) for a single incoming angle. Using fluxes, the result looks like

$$\rho_{dh}|\tau_{dh} = \frac{1}{P_i}\int dP_{r|t}, \tag{3}$$

which can be rewritten using the definition of the BSDF in Eq. 2 as

$$\rho_{dh}|\tau_{dh}(\theta_i,\phi_i) = \int B(R|T)DF(\theta_i,\phi_i,\theta_t,\phi_t)\cos(\theta_t)d\Omega_t, \tag{4}$$

where the integration covers over all solid angles in the outgoing hemisphere. The direct-hemispherical transmittance is the value ideally measured with an integrating sphere.

It is common to explicitly write the spherical coordinates, which for transmittance gives

$$\tau_{dh}(\theta_i, \phi_i) = \int_0^{2\pi} \int_0^{\pi/2} \mathrm{BTDF}(\theta_i, \phi_i, \theta_t, \phi_t) \cos(\theta_t) \sin\theta_t d\theta_t d\phi_t \quad (5)$$

$$\equiv \frac{1}{2} \int_0^{2\pi} \int_0^{\pi/2} \mathrm{BTDF}(\theta_i, \phi_i, \theta_t, \phi_t) \sin 2\theta_t d\theta_t d\phi_t. \quad (6)$$

For the special case of measurements of samples with no ϕ_t-dependence (isotropic samples) at normal angle of incidence, Eq. 6 can be rewritten as

$$\tau_{dh}^{\mathrm{iso}} = \pi \int_0^{\pi/2} \mathrm{BTDF}(\theta_t) \sin 2\theta_t d\theta_t, \quad (7)$$

where the superscript *iso* is used to point out the circular symmetry of the scattering and the $\mathrm{BTDF}(\theta_t)$ is the BTDF for light incident at normal angle.

2.2 Integrating sphere measurements

The instrument used in this paper is a Perkin–Elmer Lambda 950 spectrophotometer fitted with a Labsphere 150 mm integrating sphere. In principle any setup can be used as long as the detector, in this case the sphere port, has a finite size and can be moved relative to the sample.

A schematic drawing of the modified sample compartment is shown in Fig. 2. Two alterations have been carried out, a rail has been added, denoted 2 in Fig. 2, upon which a carriage holding the sample will slide. Also, the original 20 mm diameter sample holder plate had to be modified so that the carriage could slide to a position where the sample was in contact with the port.

The relevant part is the area of the rail and entrance port. The coordinate system used in the calculations is shown in Fig. 3.

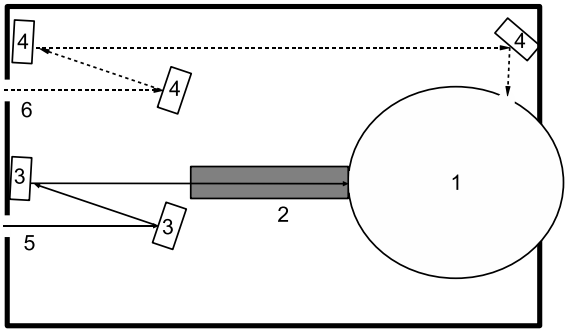

Fig. 2. Schematic drawing of the Labsphere sample compartment. 1. The integrating sphere. 2. Rail installed so that the sample can be positioned at different distances from the entrance port. 3. Mirrors focusing the sample beam. 4. Mirrors focusing the reference beam. 5 Incoming sample beam (the light generation system outside of this box is not shown.) 6. Incoming reference beam.

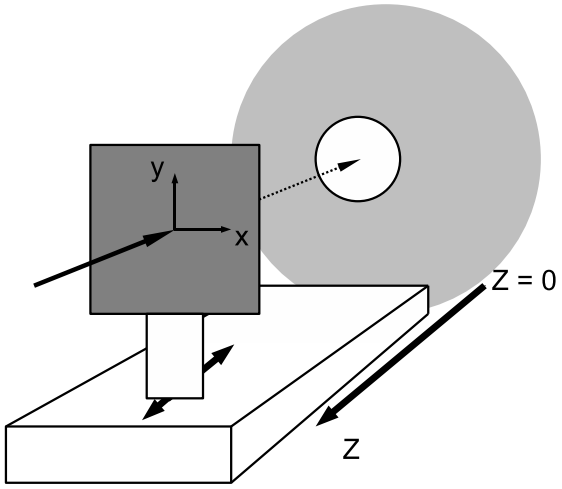

Fig. 3. Definition of the coordinate system used. The sample is moved along the z-axis, $z = 0$ means that the sample is in contact with the sphere. Increasing positive z means means that the sample moves away from the entrance port. The origin of the xy-plane is defined by the center of the entrance port.

2.3 Interpretation of measured signal

Only light transmitted in a limited scattering angle range is detected when the transmittance is measured with the sample at some distance from the entrance port. The transmittance measured at a certain distance, $T(z)$, is obtained by integrating the sample BTDF over the limited angle range that gives the sphere opening at that distance. The simplest case is with the sample in contact with the port which results in Eq. 4 with $\theta_i = \phi_i = 0$. In the following equations we therefore let the symbol θ represent θ_t since we know that $\theta_i = 0$.

Contribution from high angle scattering decreases as the sample is moved away from the port. For a point-like illumination aligned with the center of the sphere port, the decrease would be easy to model by simply limiting the upper θ bound. However, most spectrophotometers have a larger than point-like illumination size. This is usually an intended design choice since scattering samples usually are inhomogeneous to some extent and a larger illumination is wanted to obtain a representative average for the sample. Two different illumination cases are shown in Fig. 4.

It is complicated to describe the integration angle limits for light that illuminates the sample off the z-axis. An alternate approach is to add an *acceptance factor*, ψ, that depends on θ and the distance from the z-axis. The purpose of this acceptance factor is to describe how large part of the transmitted light that will be detected by the sphere. It is important to note that the acceptance is for a single angle, not all angles smaller than θ.

The fraction of light entering the sphere can be calculated [10] using the

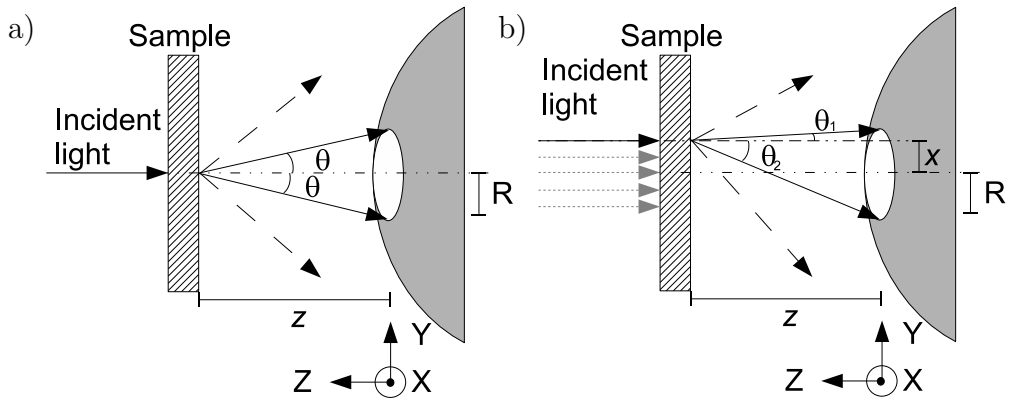

Fig. 4. Point-like illumination is demonstrated in a) and a larger illumination similar to that seen in spectrophotometers in b). With the sample at a distance z from the sphere port some light, marked with dashed arrows, will be scattered outside the port, hence not being detected.

geometry shown in Fig. 5 to be

$$\psi(d,r) = \begin{cases} 0 & \text{if} \quad |d-r| > R \\ 1 & \text{if} \quad d+r < R \\ \frac{1}{\pi}\arccos\left(\frac{r^2+d^2-R^2}{2rd}\right) & \text{otherwise.} \end{cases} \tag{8}$$

The distance d describes the distance from the z-axis, R is the radius of the sphere port, and r describes the radius of a scattering cone shell. The relationship between r and θ is $r = z\tan\theta$, where z is the distance from the sample

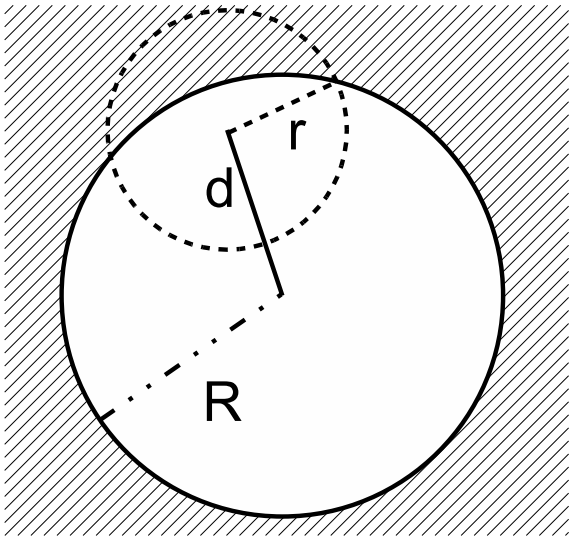

Fig. 5. The geometry for a point-like beam that strikes the sample at distance d from the center off an axis going through the center of a circular port with radius R. Light scattered a distance r is only partially inside the port.

to the sphere as shown in Fig. 3. Substitute r with z and θ in Eq. 8 then gives

$$\psi(d, z\tan(\theta)) = \begin{cases} 0 & \text{if} \quad |d - z\tan(\theta)| > R \\ 1 & \text{if} \quad d + z\tan(\theta) < R \\ \frac{1}{\pi}\arccos\left(\frac{z^2\tan^2\theta + d^2 - R^2}{2dz\tan\theta}\right) & \text{otherwise.} \end{cases} \tag{9}$$

Equation 9 gives the fraction of light scattered at an angle θ from a distance d off the z-axis axis that is detected. Hence, there will be $1 - \psi(d, z\tan(\theta))$ light scattered from that point at exactly the angle θ that is not detected. It is important to note that the equation gives no information about the amount of light scattered at the given θ, only how large a fraction of it that is detected.

The parameter d is dependent of the shape of the illuminating spot which is expected to be constant for all measurements. It is therefore possible, and wanted, to get an integrated value for ψ over all values of d. The original method for this [10] was to divide the light patch into n individual pixels and make a mean value for all pixels according to

$$\psi(z\tan(\theta)) = \frac{1}{n}\sum_i \psi(d_i, z\tan(\theta)), \tag{10}$$

but an integration will also solve the problem

$$\psi(z\tan(\theta)) = \frac{1}{A}\int \psi(d, z\tan(\theta))dS, \tag{11}$$

where A is the area of the illuminated spot and the integration is carried out over the whole area. If the intensity variation of the light spot is known this can easily be incorporated into the equation by introducing a weight term for each d.

2.4 Obtaining the BTDF

To conclude, the measured signal T is related to the BTDF by

$$T(z) = \pi\int_0^{\pi/2} \psi(z\tan\theta)\mathrm{BTDF}(\theta)\sin 2\theta\, d\theta, \tag{12}$$

where ψ is given by Eq. 11. Note that ψ is a known function, although it has to be evaluated numerically. Eq. 12 is an integral equation with the BTDF as unknown.

To solve Eq. 12 numerically, let z_i, $i = 0, \ldots, m$, denote the $m + 1$ points for which $T(z_i)$ is measured and let $\theta_j = jh$, $j = 0, \ldots, n$, be a subdivision of

the interval $0 \leq \theta \leq \pi/2$. Here, $h = \pi/2n$ and n is a positive integer. In this paper, $n = 90$ is used.

By approximating the integral in Eq. 12 by the trapezoidal rule and requiring the equality to be true for $z = z_i$, $i = 0, \ldots, m$, the following linear system of $m + 1$ equations

$$T(z_i) = \pi \sum_{j=0}^{n} \psi(z_i \tan\theta_j) \mathrm{BTDF}_j \sin 2\theta_j \, w_j \, h, \quad i = 0, \ldots, m, \tag{13}$$

in $n+1$ unknowns BTDF_j is obtained, where BTDF_j approximates $\mathrm{BTDF}(\theta_j)$. Here, w_j are the quadrature weights of the trapezoidal rule, given by $w_0 = w_n = 1/2$ and $w_j = 1$, $j = 2, \ldots, n-1$.

Using standard linear algebra notation, Eq. 13 has the form

$$Ax = b, \tag{14}$$

where the matrix A has elements $A_{i+1,j+1} = \pi \, \psi(z_i \tan\theta_j) \sin 2\theta_j \, w_j \, h$, x is the vector of unknowns, $x_{j+1} = \mathrm{BTDF}_j$, and b is the right hand side containing measured data, $b_{i+1} = T(z_i)$.

If $m = n$, A is a square matrix, but if $m \neq n$, Eq. 14 is either over- or under-determined and a unique solution does not in general exist. However, one can still compute a solution in the sense of least squares, that is, the vector x that minimizes $||Ax - b||_2$. This vector satisfies the normal equations

$$A^T A x = A^T b, \tag{15}$$

although more numerically stable methods are recommended for actually computing x.

Unfortunately, Eq. 14 cannot be solved directly using standard mathematical software. The reason is the following: Equation 12 is an integral equation of Fredholm's first kind, which is a classical example of an ill-posed problem. The solution is therefore extremely sensitive to perturbations in given data, and the same property is inherited by Eq. 14, yielding a severely ill-conditioned coefficient matrix A. Any noise in the right hand side b completely destroys the solution x.

The remedy is to regularize the problem and the most common and well-known method is the one known as Tikhonov regularization [11,12]. The idea is to compute the vector x that minimizes

$$F_\varepsilon(x) = ||Ax - b||_2^2 + 2\varepsilon ||Dx||_2^2, \tag{16}$$

where $\varepsilon > 0$ is a regularization parameter and D is a $(n+1) \times (n+1)$ matrix that poses extra constraints on the solution. One way of imposing regularity on

the solution is to choose D as a finite difference approximation of a differential operator. Forcing $||Dx||_2$ to become small then smoothens the solution. In this paper,

$$D = \begin{pmatrix} 0 & 0 & & & 0 \\ h^{-2} & 1-2h^{-2} & h^{-2} & & \\ & \ddots & \ddots & \ddots & \\ & & h^{-2} & 1-2h^{-2} & h^{-2} \\ 0 & & & 0 & 0 \end{pmatrix}, \tag{17}$$

that is, a finite difference approximation of $1 + d^2/d\theta^2$ at all inner points.

The minimizer of Eq. 16 does not satisfy $Ax = b$, not even when $m = n$. Instead, balance between a small $||Ax - b||_2$ and a small $||Dx||_2$ is sought. If ε is large, $||Dx||_2$ is forced to become small, implying smoothness in x and damping of noise. For ε small, the minimizer is closer to satisfying $Ax = b$, with the cost of less smoothening.

To derive an algorithm for computing the minimizer, note that

$$\begin{aligned} F_\varepsilon(x) &= (Ax - b)^T(Ax - b) + 2\varepsilon(Dx)^T Dx \\ &= x^T A^T Ax - 2x^T A^T b + b^T b + 2\varepsilon x^T D^T Dx. \end{aligned} \tag{18}$$

Differentiating and requiring the derivatives to be equal to zero,

$$\nabla F_\varepsilon(x) = 2A^T Ax - 2A^T b + 2\varepsilon D^T Dx = 0, \tag{19}$$

gives

$$\left(\varepsilon D^T D + A^T A\right) x = A^T b. \tag{20}$$

This is a regularized extension to the normal equations, and the set of equations that is solved when computing x, and hence BTDF, in this paper. A numerically stable algorithm for this is given at the end of this section.

In order to compute a solution, it remains to choose the regularization parameter ε. One reasonable approach is to balance the regularization error and the perturbation error. The regularization error is caused by the fact that one minimizes $F_\varepsilon(x)$ instead of solving $Ax = b$, and the perturbation error is due to noise in b, amplified by the ill-conditioning of A.

One way of finding a good balance is to compute the minimizer for different values of ε and plot $||Ax - b||_2$ versus $||Dx||_2$ in a log-log scale. It turns out that this curve has a characteristic L-shaped appearance with a pronounced corner, as shown in Fig. 6. It is therefore usually referred to as the L-curve.

For large values of ε, $||Dx||_2$ is forced to become small, and the error in x is dominated by the regularization error. Therefore, $||Ax - b||_2$ is more sensitive

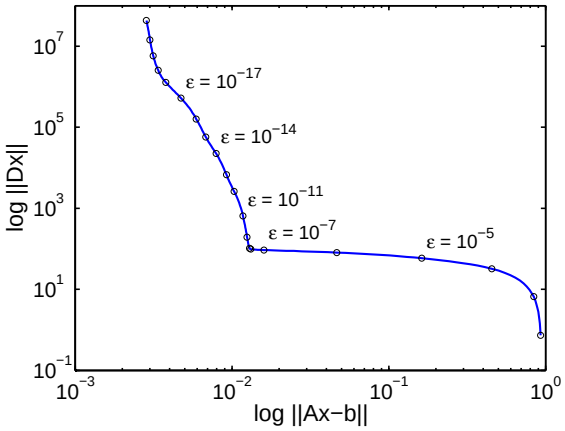

Fig. 6. The L-curve for the sample designated N73d3. Each value of the regularization paramater ε corresponds to a particular point on the L-curve. Smaller values, correponding to less smoothing, can be found att the top left corner of the picture, and larger values, corresponding to more smoothing, are located at bottom right corner. A value of $\varepsilon = 10^{-9}$ gives the balanced solution in the corner.

to changes in the regularization parameter than $||Dx||_2$ is. Consequently, large values of ε correspond to the horizontal part of the L-curve.

For small values of ε, corresponding to the vertical part of the L-curve, the opposite holds: The error is dominated by the perturbation error and $||Dx||_2$ is the most sensitive to changes in the regularization parameter.

It turns out that the corner of the L-curve gives a good balance between the regularization and perturbation errors, and this is how ε is chosen in this paper. A more general and thorough discussion on how to choose the regularization parameter is given by Hansen [13].

Once again, solving Eq. 20 is a numerically delicate affair and one should use a numerically stable method. One such approach uses the QR factorization of the augmented matrix

$$\bar{A} = \begin{pmatrix} A \\ \sqrt{2\varepsilon}D \end{pmatrix}.$$

The QR factorization produces an $(m+n+2)\times(m+n+2)$ orthogonal matrix Q and an $(m+n+2)\times(n+1)$ matrix R such that $\bar{A} = QR$. Here,

$$R = \begin{pmatrix} R_0 \\ 0 \end{pmatrix},$$

where R_0 is upper triangular and of size $(n+1)\times(n+1)$. From the definition of the 2-norm, $F_\varepsilon(x)$ given by Eq. 16 satisfies $F_\varepsilon(x) = ||\bar{A}x - \bar{b}||_2^2$, where $\bar{b}_i = b_i$, $i = 1, \ldots, m+1$, and $\bar{b}_i = 0$, $i = m+2, \ldots, m+n+2$. Since the 2-norm is

invariant under orthogonal transformations and Q is orthogonal,

$$F_\varepsilon(x) = ||Q^T(\bar{A}x - \bar{b})||_2^2 = ||Q^T(QRx - \bar{b})||_2^2 = ||Rx - Q^T\bar{b}||_2^2.$$

Clearly, $F_\varepsilon(x)$ is minimized when

$$R_0 x = c, \tag{21}$$

where $c_i = (Q^T b)_i$, $i = 1, \ldots, n+1$, and solving Eq. 21 gives the solution. An overview of regularization and solution methods for discrete ill-posed problems is given in the documentation of P. C. Hansen's MATLAB package *Regularization Tools* [14].

3 Experiment

The method was verified using two different goniophotometers to obtain BTDFs that could be compared to the results obtained with the novel method.

3.1 Materials studied

As example material a translucent highly transmitting daylighting material was used, this material has been thoroughly characterised [15–17] showing high transmittance and isotropic scattering and was therefore considered suitable to test the method.

Doped PMMA samples formed by injection molding with a single mold containing four uniform thickness segments, 1 mm, 2 mm, 3 mm, and 4 mm, and optically smooth surfaces, were studied. These samples were prepared by Roehm Degussa in Darmstadt, Germany using commercially available materials. Two different mold mixes were used, with identical optical grade clear PMMA molding beads (type N70) mixed with 3% and 7.3% by weight, of the same Plexiglas molding beads (1011F) which are doped with several micron diameter clear transparent cross-linked PMMA spheres. To be consistent with previously published work on these sheets, the sheets with 3% particles are called N73 and the sheets with 7.3% particles are called N77. A total of four samples where characterised in this report, 1 mm N73, 3 mm N73, 1 mm N77, and 3 mm N77.

The PMMA matrix used as bulk material has a refractive index of 1.495 at a vacuum wavelength of 633 nm (HeNe laser) which corresponds to 423 nm in the medium. The TRIMM particles used have a refractive index of 1.507 at a

vacuum wavelength of 633 nm (420 nm in medium). The size of the particles is not identical but ranges between 5–10 μm radius.

3.2 Goniophotometer measurements

A home-built goniometer type angle-resolved scatterometer has been used for the angle-resolved measurements [18]. It uses a HeNe laser at a wavelength of 633 nm as light source and a 7.5mm^2 area silicon diode detector for light collection. The radius of the goniometer is 58 cm. The scattering measurements were angle calibrated using the maximum intensity in the specular spot as zero degree angle. Measurements of scattering profiles for the diffusor sheets were carried out with varying θ-angle but fixed ϕ-angle assuming an isotropic scattering from the samples.

Measurements were also carried out with an Optronic Laboratories OL750-75MA measurement system. The light source was a 150 W tungsten halogen lamp. The incident light was made monochromatic to a wavelength of 633 nm using a single grating monochromator with a blaze of 0.5μm and 1200 g/mm. The detector was a 1 cm square silicon detector mount on a movable arm at a distance of 22 cm from the sample.

3.3 Integrating sphere measurements

A Perkin–Elmer Lambda 950 spectrophotometer with a Labsphere 150 mm diameter integrating sphere accessory was modified according to the descriptions in Sect. 2.2. A rail with a millimeter scale was installed in front of the transmittance sphere opening. The rail made it possible to move the sample from 0 mm up to 72 mm distance away from the sphere entrance. Larger distances was not possible due to the design of the carriage in combination with the focusing mirrors that are fixed in the sample compartment. that redirect the beam is obstructing movement further away from the port. Measurements were taken with a wavelength of 633 nm. The measured data is shown in Fig. 7.

The beam spot is approximately 9 mm by 17 mm at the port opening. The beam is converging, and hence should be modelled with different size and an angle of incidence distribution for different distances from the port. However, approximating the beam as fixed size and at normal angle of incidence worked well and significantly simplified the calculation of ψ.

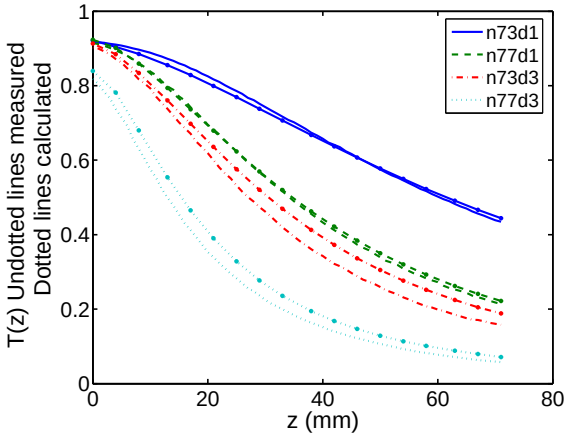

Fig. 7. Comparison between the transmittance versus distance for the four different samples. The lines without dot marks show values measured with the integrating sphere and the dotted lines are calculated from BTDF data obtained with the UTS spectrophotometer. These plotted values are the b-values used in the right hand side of Eq. 14.

4 Results and discussion

4.1 Verification of the model

Even though the goal is to find the BTDF from the measured data from the Lambda 950 it is relevant to calculate $T(z)$ using Eq. 13 and the BTDF data measured with the goniophotometers. This gives an idea what the measurements should look like to generate the correct BTDF. Figure 7 shows the $T(z)$ measured with Lambda 950 as solid lines, and $T(z)$ calculated from BTDF measurements with the UTS goniophotometer as dotted lines.

The agreement for the two thinner samples is great, the two thicker samples show a constant difference between calculation and measurement. This is probably due to the bulk-scattering properties of the samples. It is reasonable to assume that the goniometer is less sensitive to the distortion of the light beam, since the detector is further away from the sample in that case which reduces the error introduced by the assumption that the light beam does not change shape or size as it travels through the sample. It is tempting to suggest that the calculated curve is simply shifted with a length proportional to the sample thickness, that might be partially true, but the amount of bulk scattering elements would also affect such a shift. However, since such a correction would be highly sample dependent it has been left for future investigators to study.

So at first glance it looks like it should be more problematic to determine the BTDFs for the thicker samples. On the other hand, the measured data

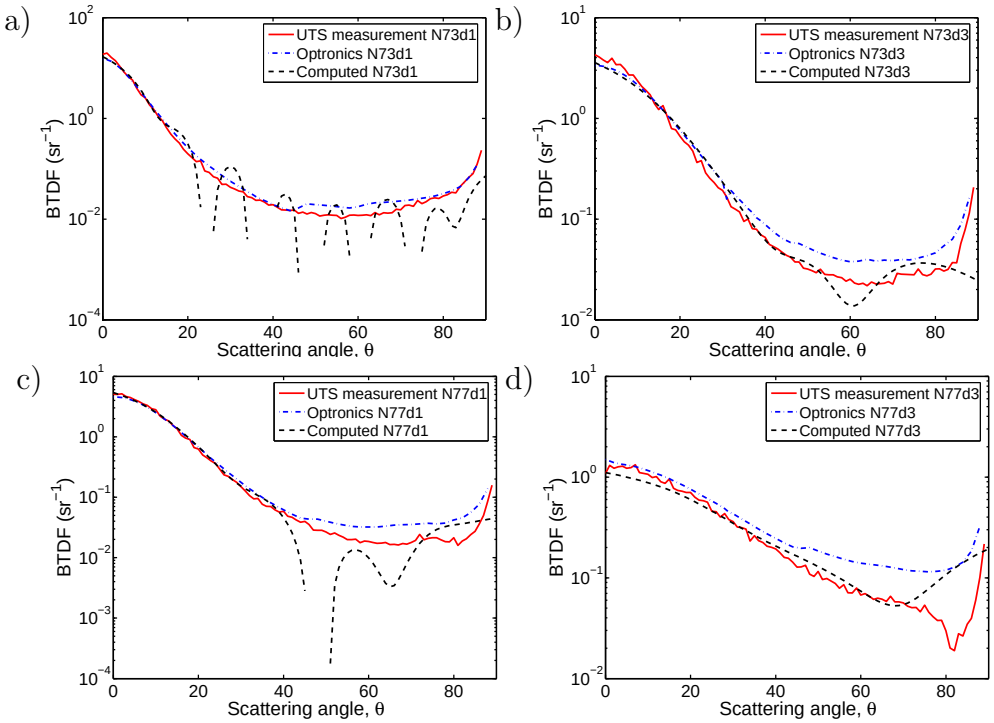

Fig. 8. The BTDFs acquired using three different methods for four different samples: a) N73d1, b) N73d3, c) N77d1, and d) N77d3. The εs used were obtained from L-curves of the individual samples as a) 10^{-12}, b) 10^{-9}, c) 10^{-10}, and d) 10^{-8}.

for the two thinner samples has not yet started to converge to the specular transmittance value. This means that there is no data to determine the BTDF exclusively for low scattering angles. This, somewhat surprisingly, does not turn out to be a problem for determining the BTDF for low angles.

The reason that data was not obtained for higher values of z in our study was due to the limited space in the sample compartment.

4.2 BTDFs obtained by solving the regularized system of equations

The BTDF for the four samples was obtained using two goniophotometers and also computed from integrating sphere measurements by solving Eq. 20. The different results are shown for each sample in Fig. 8.

The first thing to note is the good agreement between the calculated values and the measured, the difference between the two goniometers are as large as that between the goniometers and the calculated values. Except from the strong oscillations in the computational solution of the two thinner samples, and weaker oscillations that can be discerned for the thicker samples as well. Some BTDF values are below zero, which results in the discontinuities in the logarithmic graphs, clearly an unphysical solution.

As discussed in the next section, the oscillations are artifacts, generated by the solution process. There is nothing that suggests that they are due to optical interference.

Note the good agreement between the computed and measured values for small angles. This is true even for the two thinner samples where the measured data is incomplete. This is a remarkable and promising result.

4.3 Selection of optimal regularization parameter ε

As discussed in Sect. 2.4, choosing ε at the corner of the L-curve gives a good balance between the regularization and perturbation errors. As stated in Fig. 8 the values obtained by this method are 10^{-12}, 10^{-9}, 10^{-10}, and 10^{-8} for N73d1, N73d3, N77d1, and N77d3 respectively.

In Fig. 9 the solution for sample N73d1 is plotted for different values of ε. If ε is small, the ill-conditioning of the problem amplifies noise in the measured data and the highly oscillatory perturbation error dominates the solution.

If ε is large, the problem is over-regularized and the solution is smoothened to such a degree that not only the oscillating perturbation error, but also the true solution itself is damped and smeared. The solution is now dominated by the regularization error.

For some medium sized ε, there is a good balance between regularization and perturbation errors. However, also for the optimal ε, both kinds of errors are present. The perturbation error adds oscillations and the regularization error smears rapid variations.

This is probably the reason why it is more difficult to compute a good solution for the low-scattering samples. The BTDF is here a more rapidly changing curve and choosing ε large enough to efficiently damp out the oscillatory perturbation error smoothens the true solution too much. The best compromise, according to the L-curve, is to keep the oscillations seen in Fig. 8. Without any knowledge about the answer it is daring to select any other ε.

The resoning is even more clear for high-scattering samples, especially in the extreme case of Lambertian samples which have a constant BTDF. There, the true solution is extremely smooth and ε can be very large, removing all oscillations.

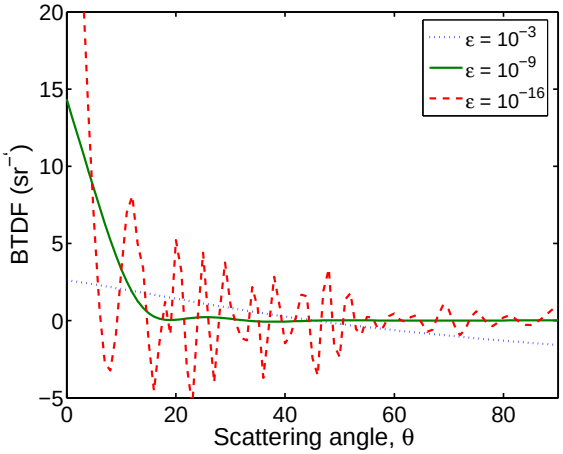

Fig. 9. The number of oscillation is reduced compared to Fig. 8a) by changing epsilon to a smaller number.

5 Conclusions

Given the presented results it is clear that a commercial spectrophotometer fitted with an integrating sphere can be used to acquire BTDF values for isotropically scattering samples. The results for low-scattering samples contained unphysical oscillations that originates from the balance between the regularization and perturbation errors in the solution. The correct value can be seen as a line that the oscillations are bound around. For more diffuse samples the solution is better, and this agrees with the understanding of the regularization error and the selection of the regularization parameter ε.

Initial analysis of possible ways of reducing the oscillations suggests that there are no simple changes that can improve the solution. It is possible that modelling or the diskretization procedure must be significantly improved, but it might also be possible to improve the experimental set-up so that more information is obtained and the solution comes out without oscillations.

There are no intrinsic constraints in this method that limits its use to transmittance at normal angle of incidence. However, modifications of a commercial instrument to be able to experimentally obtain values for reflectance and/or varying angles of incidence are considered to be of a different magnitude compared to the case that is demonstrated in this paper.

Future work to investigate is planned to determine how the calculations can be improved and what experimental parameters will need to be improved to obtain better results.

6 Acknowledgements

This work was supported by the Assistant Secretary for Energy Efficiency and Renewable Energy, Office of Building Technology, Building Technology Programs of the U.S. Department of Energy under Contract No. DE-AC03-76SF00098.

Jonas Persson, Paul Sjöberg, and Per Sundqvist at Uppsala University are acknowledged for initial discussion about solving the ill-posed system of equations. Mike Rubin is acknowledged for modifying the instrument at Lawrence Berkeley National Lab and for discussions about what could be measured with the modified instrument and for proof reading. Oliver Meier at Lawrence Berkeley National Lab was helpful building the carriage and port plates. Professor Arne Roos at Uppsala University independently suggested moving the sample away from the sphere port to obtain more information about diffuse samples.

References

[1] St. John AE, Multiple internal reflection structure in a silicon detector which is obtained by sandblasting, US Patent 3,487,223 .

[2] W. J. Platzer, The altset project: Measurement of angular properties for complex glazing, in: Proceedings of the Third International ISES Europe (Eurosun) Conference, 2000.

[3] F. E. Nicodemus, Directional reflectance and emissivity of an opaque surface, Applied Optics 4 (7) (1965) 767–773.

[4] E. L. Dereniak, L. G. Brod, J. E. Hubbs, Bidirectional transmittance distribution function measurements on ZnSe, Applied Optics 21 (24) (1982) 4421–4425.

[5] J. C. Stover, Optical Scattering : Measurement and Analysis, SPIE Press, Bellingham, 1995.

[6] ASTM E 1392-96, Standard practice for angle resolved optical scatter measurements on specular or diffuse surfaces, ASTM International.

[7] SEMI ME1392-0305, Guide for angle resolved optical scatter measurements on specular or diffuse surfaces, Semiconductor Equipment and Materials International.

[8] Commission Internationale de l'Eclairage, Radiometric and photometric characteristics of materials and their measurement, 38 (1977).

[9] P. Apian-Bennewitz, J. von der Hardt, Enhancing and calibrating a goniophotometer, Solar energy materials and solar cells 54 (1970) 309–322.

[10] J. C. Jonsson, A. Roos, G. B. Smith, Light trapping in translucent samples and its effect on the hemispherical transmittance obtained by an integrating sphere, in: Proceedings of SPIE's 48th Annual Meeting, Vol. 5192, 2003, pp. 91–100.

[11] A. N. Tikhonov, Solution of incorrectly formulated problems and the regularization method, Dokl. Akad. Nauk. SSSR 151 (1963) 501–504.

[12] A. N. Tikhonov, V. Y. Arsenin, Solutions of Ill-posed Problems, Winston & Sons, Washington, D.C., 1977.

[13] P. C. Hansen, Analysis of discrete ill-posed problems by means of the L-curve, SIAM Review 34 (1992) 561–580.

[14] P. C. Hansen, Regularization tools: a Matlab package for analysis and solution of discrete ill-posed problems, Numer. Algorithms 6 (1–2) (1994) 1–35.

[15] G. B. Smith, J. C. Jonsson, J. Franklin, Spectral and global diffuse properties of high-performance translucent polymer sheets for energy efficient lighting and skylights, Appl. Opt. 42 (19) (2003) 3981–3991.

[16] J. C. Jonsson, G. B. Smith, C. Deller, A. Roos, Directional and angle-resolved optical scattering of high-performance translucent polymer sheets for energy efficient lighting and skylights, Appl. Opt. 44 (14) (2003) 2745–2753.

[17] J. C. Jonsson, G. B. Smith, G. A. Niklasson, Experimental and Monte Carlo analysis of isotropic multiple Mie scattering, Opt. Comm. 240 (2004) 9–17.

[18] G. B. Smith, D. C. Green, G. McCredie, M. Hossain, P. D. Swift, M. Luther, Optical characterisation of materials and systems for daylighting., Renewable Energy 22 (2001) 85–90.